

Second Law Analysis in a Non-Newtonian Fluid Flow in an horizontal Channel with Narrowing and Widening

Naoufal ghouli¹, Ali Mchirgui¹, Atef El Jery^{1,2}, Mourad Magherbi^{1,3}

¹Engineers National school of Gabes, Gabes University, Tunisia.

² King Fahd University, K.S.A.

³High Institute of Applied Sciences and Technology, Gabes University, Tunisia.

Article Info

Article history:

Received Jun 1, 2023

Revised Jun 21, 2023

Accepted July 28, 2023

Keywords:

Non-Newtonian fluid,
Porous media,
channel,
irreversibility,
numerical methods

ABSTRACT

This work studies the flow of a non-Newtonian power-law fluid with viscous dissipation through a pipe with a variable expand ratio (B). The influence of the power law index (n), expand ratio (B), Darcy number (Da) and Brinkman number (Br) on heat transfer and thermodynamics irreversibility is investigated. Equations of the problem are solved numerically using COMSOL software. Results show that heat transfer and entropy generation are deeply affected by selected governing parameters. Both thermal entropy generation and average Nusselt number are maximal at low power index and at high medium permeability. Power index effect is insignificant at relatively low Darcy number. Considering viscous dissipation with high Brinkman number, heat transfer direction can be reversed at moderate Darcy number and high-power index.

This is an open access article under the [CC BY](https://creativecommons.org/licenses/by/4.0/) license.



Corresponding Author:

Ali Mchirgui,
Engineers National school of Gabes,
Gabes University,
Tunisia
Email: mchirgui@yaho.com

1. INTRODUCTION

Newton's law of viscosity is violated by non-Newtonian fluids; their viscosities depend on the stresses applied. Non-Newtonian fluid flow is known to be important in many practical applications such that food industry, oil drilling, pharmaceuticals, advanced materials manufacturing, protective equipment design, medicine etc. This illustrates the versatility of these fluids and their impact in many aspects of our daily lives from industry to scientific research. Their unique behavior offers a wide range of possibilities for innovative and practical applications. In this context, considerable interest focused on non-Newtonian fluid flow, with and without, viscous dissipation. Numerous papers have been published on this subject.

Thermal convection heat transfer to blood steadily flowing in a pipe was investigated by Dumas et al. [1], The velocity field was distributed analytically, while the temperature field was determined numerically using the finite-difference method to solve the energy equation for two thermal conditions (uniform parietal temperature and parietal heat flux density). Blackwell [2] proposed a numerical solution of Graetz problem by considering circular ducts submitted to uniform parietal temperature the viscous dissipation and axial fluid conduction were neglected. The same problem was studied by Johnston [3] taking into account the axial conduction. Basu et al. [4] explored the impact viscous dissipation on heat transfer; it

was found that viscous dissipation considerably affects the flow especially at the inlet zone. Min et al. [5,6] analytically and numerically examined the hydrodynamic and simultaneous development of laminar flow of a Bingham fluid in a cylindrical pipe. A good agreement between the digital and analytical solutions was found. non-Newtonian laminar fluid flow in a circular pipe was numerically explored by Vradis et al. [7]. Recently, Khatyr et al. [8] and Nouar [9] focused on this problem by considering impact of the dissipation function on the thermal field. Afrasiab [10] examined natural convection in a cavity saturated by a power-law fluid and heated from the bottom by heat source. He showed that increasing the Rayleigh number leads to enhancing the natural convection in the cavity which is more pronounced at shear thinning fluids ($n < 1$). Housseem and Mohamed [11] exhibited a numerical study based on the resolution of the Ostwald fluid flow equations around a heated cylinder. They pointed the presence of a recirculation zone behind the obstacle which is affected by buoyancy forces. Yazdani et al. [12] explored the effect of the power index on entropy generation in a saturated trapezoidal cavity. Tayari et al. [13] investigated created entropy in a Darcy-Brinckman inclined porous channel. They found that entropy production reaches extreme values for well-defined channel inclinations. Neffah et al. [14] studied heat and mass transfer with chemical reaction in an anisotropic porous channel saturated by a non-Newtonian fluid. Effects of the characteristic parameters of the medium and the chemical reaction were examined.

Flows in widening/shrinking pipes are important hydrodynamic phenomena, as they are present in many engineering applications. Changing the diameter of a flowing pipe leads to complex variations in fluid velocity, pressure and heat transfer, with significant impacts on the efficiency of transport systems. To better understand these flows, numerous studies have been carried out and published. Alleborn et al. [15] used a channel with sudden expansion to study the flow of an incompressible fluid. The study was developed by considering limit cases for geometric and flow parameters and by comparing numerical results with analytical solutions. Bifurcation phenomena was investigated Drikakis [16], [17] for compressible [16] and incompressible flow [17] the obtained results was in good agreement with the work by Battaglia et al. [18]. Cherdrone et al. [19] experimentally investigated asymmetrical flows that form in symmetrical geometries with sudden expansion. The specific conditions that give rise to asymmetric flow and the causes of this asymmetry were investigated. The same phenomenon was studied by Fearn et al. [20]. The study showed that the flow becomes time-dependent due to three-dimensional effects. Mahfoud et al. [21] considered the isothermal flow of a non-Newtonian fluid in a rectangular pipe with an abrupt contraction of ratio 4 at different Reynolds number values and presented correlations for axial velocity. A parallel multigrid flow solver was employed by Schreck and Schäfer [22] to study bifurcation in sudden channel expansions. The study deals with the efficiency of the numerical method and the effect of the problem geometry on the bifurcation phenomena.

To the best of our knowledge, no valuable publications about fluid flows including the non-Newtonian character, presence of singularities and the existence of viscous dissipation have been confronted. In this perspective, this work is carried out in order to study a power law fluid flow, subjected to viscous dissipation, through a pipe with variable expand ratio.

II. Mathematical formulation

The system under consideration consists of a non-Newtonian fluid flowing through a narrowing-widening porous channel. The channel is of length L , and the widened and narrowed channels are of height H and H' respectively. The channel has an aspect ratio of $A=L/H$ (the ratio of the total length of the channel to the height of the wide pipe) and an expand ratio of $B=H'/H$, defined as the ratio of the height of the narrowed section to that of the wide section. The narrowing is not abrupt, so the two compartments (wide and narrowed) are linked by sloping walls at an angle (α) to the horizontal. Only the upper and lower walls of the wide parts of the channel are heated. The remaining walls are assumed to be adiabatic. The fluid enters from the left with a constant cold temperature T_c and a constant horizontal velocity U_0 . The characteristics of the channel studied are shown in figure 1. The aspect ratio A is considered to be constant and equal to 6, while the expand ratio takes the values 0.75, 0.5 and 0.25. The narrowed channel length is constant, so that a variation in the B -ratio systematically induces a variation in the angle of inclination (α such that $\tan(\alpha) = 1-B$) of the inclined wall.

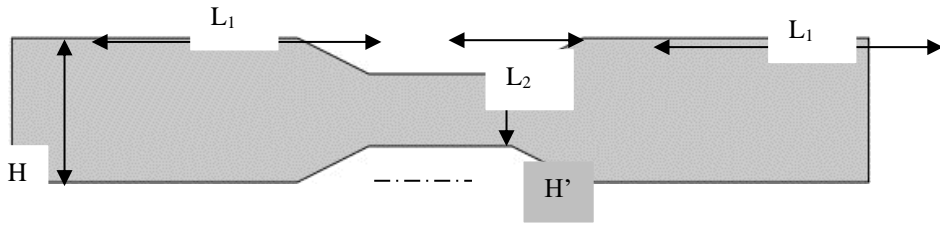
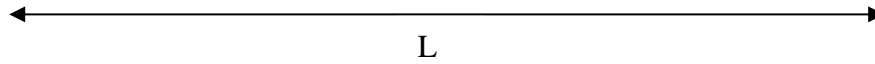


Figure 1: Geometry of the studied channel α



Following Shenoy [13] and Neffah et al. [5], conservation equations of mass, momentum and energy are respectively:

$$\frac{\partial u}{\partial x} + \frac{\partial v}{\partial y} = 0 \tag{1}$$

$$\frac{\rho}{\varepsilon^2} \left(u \frac{\partial u}{\partial x} + v \frac{\partial u}{\partial y} \right) = -\frac{\partial p}{\partial x} + \frac{1}{\varepsilon^n} \frac{\partial \tau_{xx}}{\partial x} + \frac{1}{\varepsilon^n} \frac{\partial \tau_{xy}}{\partial y} - \frac{\mu^*}{k^*} |V|^{n-1} u - \rho g \sin \beta \tag{2}$$

$$\frac{\rho}{\varepsilon^2} \left(u \frac{\partial v}{\partial x} + v \frac{\partial v}{\partial y} \right) = -\frac{\partial p}{\partial y} + \frac{1}{\varepsilon^n} \frac{\partial \tau_{yy}}{\partial y} + \frac{1}{\varepsilon^n} \frac{\partial \tau_{yx}}{\partial x} - \frac{\mu^*}{k^*} |V|^{n-1} v - \rho g \cos \beta \tag{3}$$

$$\rho C_p \left(u \frac{\partial T}{\partial x} + v \frac{\partial T}{\partial y} \right) = k \left(\frac{\partial^2 T}{\partial x^2} + \frac{\partial^2 T}{\partial y^2} \right) + \mu^* \left(2 \left(\frac{\partial U}{\partial X} \right)^2 + 2 \left(\frac{\partial V}{\partial Y} \right)^2 + \left(\frac{\partial U}{\partial Y} + \frac{\partial V}{\partial X} \right)^2 \right) \tag{4}$$

$$\text{With: } |V| = \sqrt{u^2 + v^2} \tag{5}$$

The power law model stress tensor is :

$$\bar{\tau} = \mu^* |\dot{\gamma}|^{n-1} \dot{\gamma} \tag{6}$$

with

$$\dot{\gamma} = \nabla \vec{V} + (\nabla \vec{V})^T \text{ and } |\dot{\gamma}| = \sqrt{\frac{\sum \sum \dot{\gamma}_{ij} \dot{\gamma}_{ij}}{2}} \tag{7}$$

$$\tau_{xx} = 2\eta \frac{\partial u}{\partial x}; \tau_{yy} = 2\eta \frac{\partial v}{\partial y}; \tau_{yx} = \tau_{xy} = \eta \left(\frac{\partial v}{\partial x} + \frac{\partial u}{\partial y} \right) \tag{8}$$

$$\eta = \mu^* \left(2 \left(\frac{\partial u}{\partial x} \right)^2 + 2 \left(\frac{\partial v}{\partial y} \right)^2 + \left(\frac{\partial v}{\partial x} + \frac{\partial u}{\partial y} \right)^2 \right)^{\frac{n-1}{2}} \tag{9}$$

By using the dimensionless variables below:

$$X = \frac{x}{H}; Y = \frac{y}{H}; P = \frac{H^2 p}{\rho \alpha^2}; U = \frac{u}{\varepsilon U_i}; V = \frac{v}{\varepsilon U_i}; \theta = \frac{T - T_c}{T_H - T_c} \tag{10}$$

The governing dimensionless equations are:

$$\frac{\partial U}{\partial X} + \frac{\partial V}{\partial Y} = 0 \tag{11}$$

$$U \frac{\partial U}{\partial X} + V \frac{\partial U}{\partial Y} = -\frac{\partial P}{\partial X} + \frac{\partial}{\partial X} \left(\frac{2\chi}{Re} \left(\frac{\partial U}{\partial X} \right) \right) + \frac{\partial}{\partial Y} \left(\frac{\chi}{Re} \left(\frac{\partial U}{\partial Y} + \frac{\partial V}{\partial X} \right) \right) - \frac{1}{Re Da^{\frac{n+1}{2}}} |V|^{n+1} U + \tag{12}$$

$$U \frac{\partial V}{\partial X} + V \frac{\partial V}{\partial Y} = -\frac{\partial P}{\partial Y} + \frac{\partial}{\partial Y} \left(\frac{2\chi}{Re} \left(\frac{\partial V}{\partial Y} \right) \right) + \frac{\partial}{\partial X} \left(\frac{\chi}{Re} \left(\frac{\partial V}{\partial X} + \frac{\partial U}{\partial Y} \right) \right) - \frac{1}{Re Da^{\frac{n+1}{2}}} |V|^{n+1} V + \tag{13}$$

$$U \frac{\partial \theta}{\partial X} + V \frac{\partial \theta}{\partial Y} = \frac{1}{\varepsilon Re Pr} \left(\frac{\partial^2 \theta}{\partial X^2} + \frac{\partial^2 \theta}{\partial Y^2} \right) + \frac{Br^*}{Pe} \left(2 \left(\frac{\partial U}{\partial X} \right)^2 + 2 \left(\frac{\partial V}{\partial Y} \right)^2 + \left(\frac{\partial U}{\partial Y} + \frac{\partial V}{\partial X} \right)^2 \right)^{\frac{n+1}{2}} \tag{14}$$

The dimensionless parameters involved in the above equations are:

$$Re = \frac{\rho H^n U_i^{2-n}}{\mu^*}, Da = \frac{\left(\frac{k^*}{\varepsilon^n} \right)^{\frac{2}{n+1}}}{H^2}, Pr = \frac{\mu^* C_p \left(\frac{U_i}{H} \right)^{n-1}}{k}, Ra = \frac{\rho g \beta_T \Delta T H^{2n+1}}{\alpha^n \mu^*}, Br^* = \frac{\mu^* U_i^{n+1}}{k \Delta T H^{n-1}} \tag{15}$$

$$\chi = \left[2 \left(\frac{\partial U}{\partial X} \right)^2 + 2 \left(\frac{\partial V}{\partial Y} \right)^2 + \left(\frac{\partial V}{\partial X} + \frac{\partial U}{\partial Y} \right)^2 \right]^{\frac{n-1}{2}} \tag{16}$$

III. Entropy generation

By using the transformations in Eq.10, the dimensionless total entropy production expression becomes [14]:

$$S_{tl} = \left(\left(\frac{\partial \theta}{\partial X} \right)^2 + \left(\frac{\partial \theta}{\partial Y} \right)^2 \right) + \frac{Br^* \Omega_1 \Phi}{Da^*} (U^2 + V^2) + Br^* \Omega_2 \left(2 \left(\frac{\partial U}{\partial X} \right)^2 + 2 \left(\frac{\partial V}{\partial Y} \right)^2 + \left(\frac{\partial U}{\partial Y} + \frac{\partial V}{\partial X} \right)^2 \right)^{\frac{n+1}{2}} \quad (17)$$

$$\text{Where } Br^* = \frac{\mu^* U_i^{n+1}}{k \Delta T H^{n-1}}, \Omega_1 = \frac{T_0}{\Delta T} \varepsilon^{\frac{n+1}{2}} \text{ and } \Omega_2 = \frac{T_0}{\Delta T} \varepsilon^{n+1} \quad (18)$$

In Eq. (13), the first term is the thermal irreversibility (S_{th}). The second and the third traduce respectively the Darcy (S_{dv}) and viscous (S_{fv}) irreversibilities. They are given by:

$$S_{th} = \left(\frac{\partial \theta}{\partial X} \right)^2 + \left(\frac{\partial \theta}{\partial Y} \right)^2 \quad (19)$$

$$S_{dv} = \frac{Br^* \Omega_1 \Phi}{Da^*} (U^2 + V^2) \quad (20)$$

$$S_{fv} = Br^* \Omega_2 * \left(2 \left(\frac{\partial U}{\partial X} \right)^2 + 2 \left(\frac{\partial V}{\partial Y} \right)^2 + \left(\frac{\partial U}{\partial Y} + \frac{\partial V}{\partial X} \right)^2 \right)^{\frac{n+1}{2}} \quad (21)$$

The dimensionless total created entropy is the integral of Eq.17, over the entire channel.

$$S_T = \iint_{00}^{1 L/H} S_{t,l} dx dy \quad (22)$$

The mean Nusselt number at the bottom hot wall is :

$$Nu_m = -\frac{1}{L} \int_0^L \frac{\partial \theta}{\partial Y} dx \quad (23)$$

IV. Numerical procedure

By considering the opted boundary and initial conditions, a COMSOL numerical code was established in order to solve the governing dimensionless equations. COMSOL Multiphysics use F.E.M. method to discretize the governing equations of the flow and create the numerical model in space. This method is well suited to modeling and simulating complex problems involving several physical phenomena. To solve this system of equations, COMSOL uses advanced numerical methods such as the conjugate gradient method, Newton-Raphson method, or other iterative solving techniques. To test the accuracy of the present work the found results were validated with those obtained by a FORTRAN code previously developed by members of our Laboratory at the National Engineering School of Gabès-Tunisia (Magherbi et al. [11], Tayari et al. [4]) and with other published work, in the case of a channel with expand ratio equal to unity. Tables 1 and 2 give maximum dimensionless velocity component and averaged Nusselt number compared with other results respectively. As can be seen, our results agree well with those reported in the literature.

Table 1 : Maximum of x-velocity component (Pr=0.70, Re=100)

1e-9	-----	1.020	1.010	-----
0.001	1.080	1.060	1.060	1.090
0.01	1.170	1.230	1.110	1.300
0.05	1.330	1.400	1.260	-----
0.1	1.410	1.440	1.330	1.550

Table 2 : Mean Nusselt number (Pr=0.70 , Re=1.0)

0.01	101.25	100.324	99.936	103.35
0.05	21.532	21.193	21.213	22.119
0.1	11.227	10.785	11.098	11.587

V. Results and discussion

Due to considerable number of variables and operating parameters, we have limited our work to the influence of the power law index (n), expand ratio (B), Brinkman (Br) and Darcy (Da) numbers on the flow. In this same context, we have neglected the viscous contributions to the thermodynamics irreversibility (in Eq.17), and accordingly the total created entropy (S_T) is reduced only to the thermal cause (S_{th}).

V.1. Effect of the power law index and expand ratio.

In this section, Pr, Re and Da are fixed to 70, 50 and 10^{-3} , respectively. Figure2 illustrates the variation of (S_T) and (Nu_m) versus power law index for different expand ratio. In absence of heating by

viscous dissipation effects one can see that thermal created entropy and Nusselt number are two relatively close quantities.

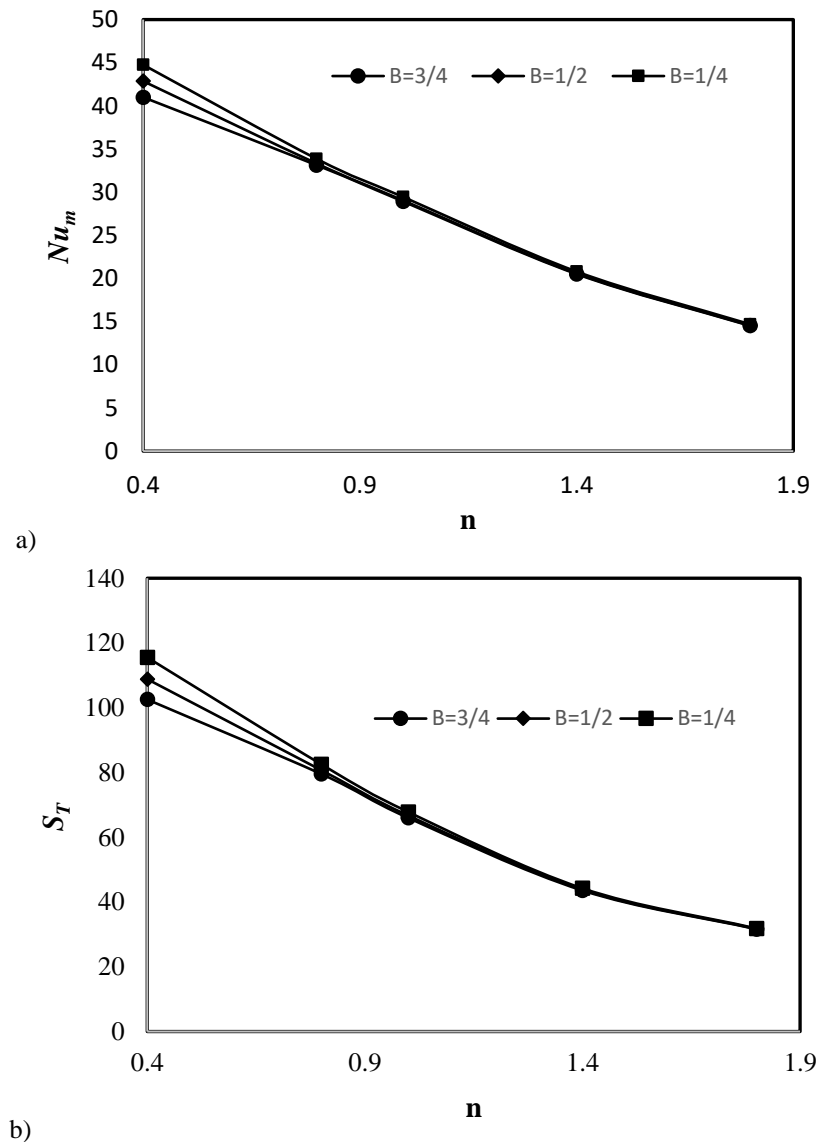


Figure 2 : Variation of: a) Nu_m ; b) S_T with the power-index for selected expand ratios ($Da=10^{-3}$, $Pr=70$ et $Re=50$)

As seen in Fig.2a, For constant B , Nu_m is maximal for shear-thinning fluid ($n=0.4$). For given shear rate, the apparent viscosity of the non-Newtonian fluid diminishes when n decreases. Therefore, at low n , the viscous forces are weak and then do not affect the inertial forces and the convection motion. In this case, thermal gradients are significant, generating important heat transfer and thermal irreversibility (Fig.2a-b). It is observed that Nu_m decreases as n rises and tends towards a minimum value at high n . This result is consistent with the work of Afrasiab [10]. Certainly, increasing the power index (from 0.4 to 1.8) leads to a raise of the fluid apparent viscosity at given shear rate. When increasing n , non-Newtonian fluid character progress from a shear thinning to a shear thickening one, which leads to a raise of the fluid apparent viscosity. Thus, it becomes more difficult to move which reduces convection phenomenon and consequently heat transfer and entropy generation decrease. Note that the decrease of Nu_m with n is noteworthy. By way of indication and for an aspect ratio $B=3/4$, the reduction in the production of thermal entropy is 66% when n varies from 0.4 to 1.8. Additionally, and for fixed n , one can see from Fig.2 that the influence of the expand ratio B on Nu_m and S_T is highly significant for shear-thinning fluid, slight for Newtonian fluids and almost absent for shear thickening fluids ($n>1$). In this context, we estimate a decrease in entropy production equal to 12%, 2% and 0.7% for a power index equal to 0.4, 1 and 1.8 respectively when the aspect ratio is increased from 0.25 to 0.75.

In order to better observe heat exchanges between the fluid and the active channel walls (wide part), the isotherms for $n=0.4$ and 1.8 are shown in figure 3. In the case of a shear thinning fluid ($n=0.4$), Fig.3.a shows the appearance of a thermal boundary layer reflecting significant heat transfer between the fluid and the hot walls of the two wide compartments. Thermal gradients are significant, giving rise to significant Nusselt number and entropy production. Note that isotherms in the vicinity of the hot walls of the left-hand compartment are tighter than those of the right-hand compartment, indicating more intense heat transfer and irreversibilities in this region of the pipe.

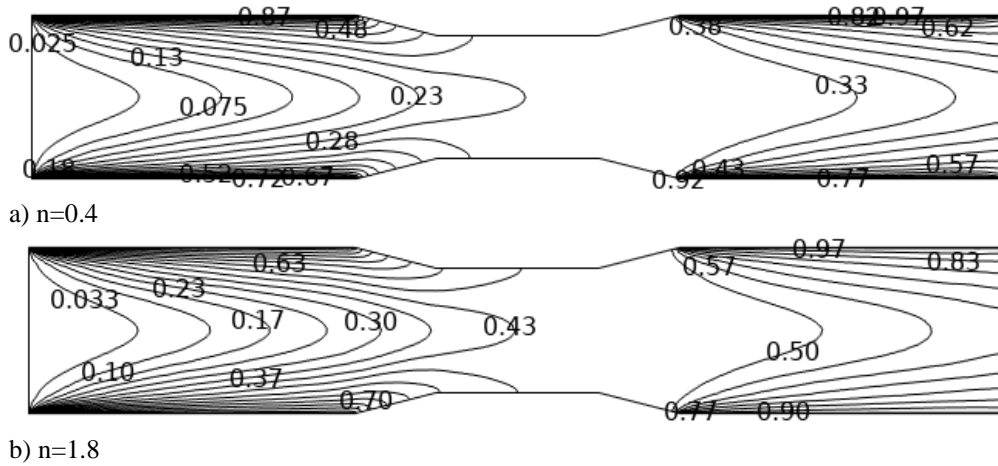


Figure 3 : Isotherms variation with the power-index for selected aspects ratios ($Da=10^{-3}$, $Pr=70$ et $Re=50$)

As we increase n (Fig.3b), we see a spreading of the isotherms at the hot wall levels for both compartments, heralding a reduction in thermal gradients and consequently a simultaneous decrease in Nu_m and S_T . The absence of thermal gradients in the shrunken central part induces the absence of heat transfer and therefore of entropy production in this part. One can note that, for shear thinning fluid most of the thermal energy received by the fluid is conveyed in the longitudinal direction (direction of flow). Whereas for $n=1.8$, part of this energy is transversely transmitted to the core of the fluid. This can be explained by the fact that by increasing the power index to 1.8 , the viscosity of the fluid becomes significant, inducing the increase of viscous friction forces and a reduction in inertia forces. Thus, heat transfer by conduction becomes more significant in the transverse direction leading to an increase in fluid temperature at the center of the flow. This result is clearly illustrated by Fig. 4, giving evolution of local fluid temperature along the channel axis (in $y=0.5$) for $n=0.4, 1$ and 1.8 .

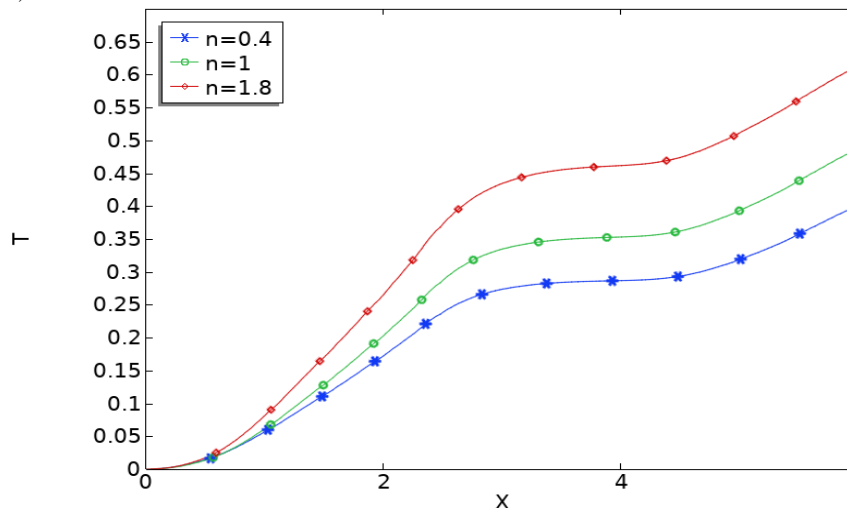


Figure 4 : Variation of local temperature along x-coordinate at $y=0.5$ for selected power-index ($Da=10^{-3}$, $Pr=70$ et $Re=50$)

Note from this figure that the temperature at the center of the flow increases as soon as the fluid enters the wide hot part of the channel where it receives heat from the top and bottom heated pipe walls. At the narrowed adiabatic part, the temperature of the fluid remains quasi-constant before increasing again while penetrating in the wide straight heated part of the channel.

V.2. Effect of the power law index and Darcy number.

Fig. 5 illustrates the effect of n and Da on Nu_m calculated on the bottom active channel walls (Fig.5.a) and S_T inside the entire channel (Fig.5.b). A similar behavior of created entropy generation and mean Nusselt number is obtained.

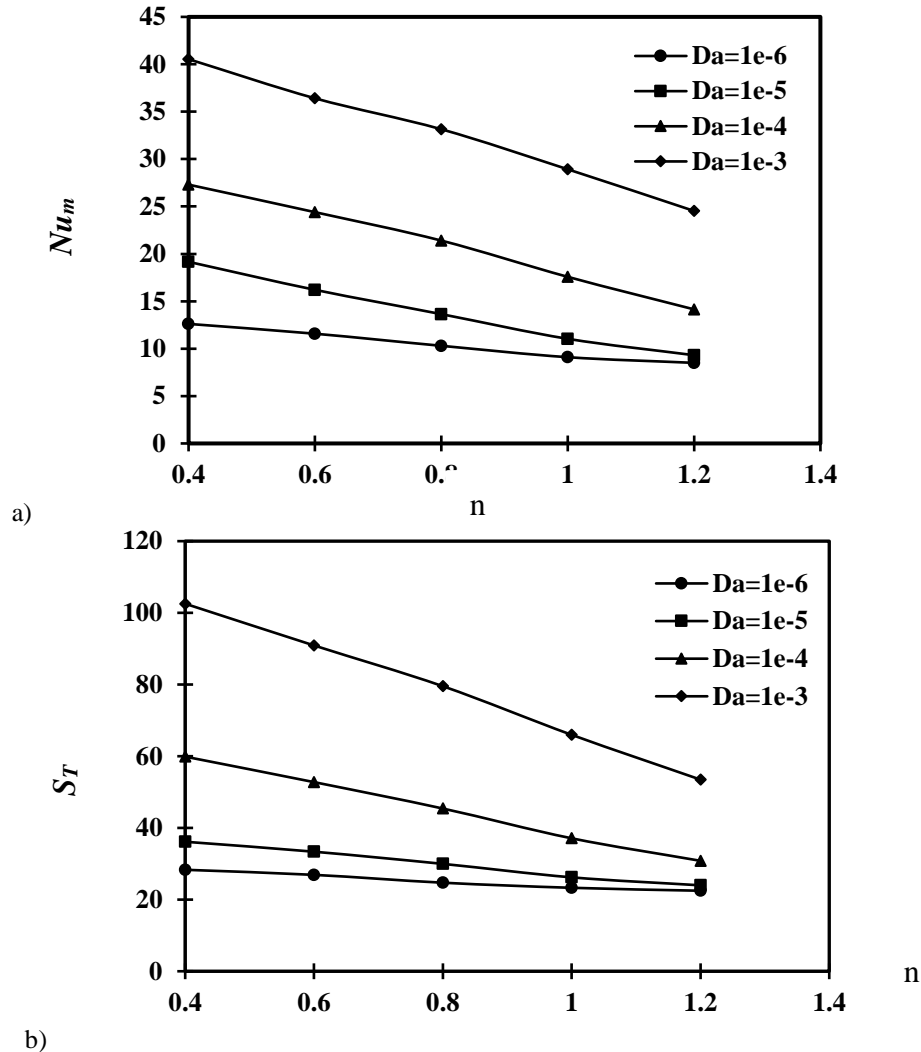


Figure 5: Variation of : a) Nu_m ; b) S_T with the power-index for selected Darcy number. (Pr=70 et Re=50, Br=0 ;B=0.75)

As it can be seen, for low Da ($\leq 10^{-6}$), the power index has no significant effect on Nu_m . In fact, low permeability of the porous medium reduces fluid mobility thus, convection effects are insignificant in favor of a dominance of transverse heat transfer conduction between the hot walls and the non-Newtonian fluid. In this context, the system is compared to a solid matrix, and consequently a variation in the power index remains with no appreciable effect on the flow. As Darcy number increases, effect of power index on Nusselt number becomes more important. A decrease in Nu as the power index increases is obtained i.e., from thinning to thickening behavior. For shear-thickening fluids ($n > 1$), fluid viscosity increases with shear rate, especially near the walls of the system under study. This will generate an increase in viscous forces, which in turn will decelerate the fluid and reduce heat transfer as well as entropy production. We can conclude that an increase in (n) has a similar, but less significant, effect than a decrease in Da . It should also be noted that the greater the Da , the greater the decrease in Nu . In this context, we can cite a decrease in Nu of almost 40% when n goes from 0.4 to 1.2. The effect of Da is more significant, in terms of heat transfer and thermodynamic irreversibility, for shear-thinning fluids. By way of example, Fig. 5b shows an increase in entropy production of almost 70% for $n=0.4$ versus 50% for $n=1.2$ when Da is increased from 10^{-6} to 10^{-3} .

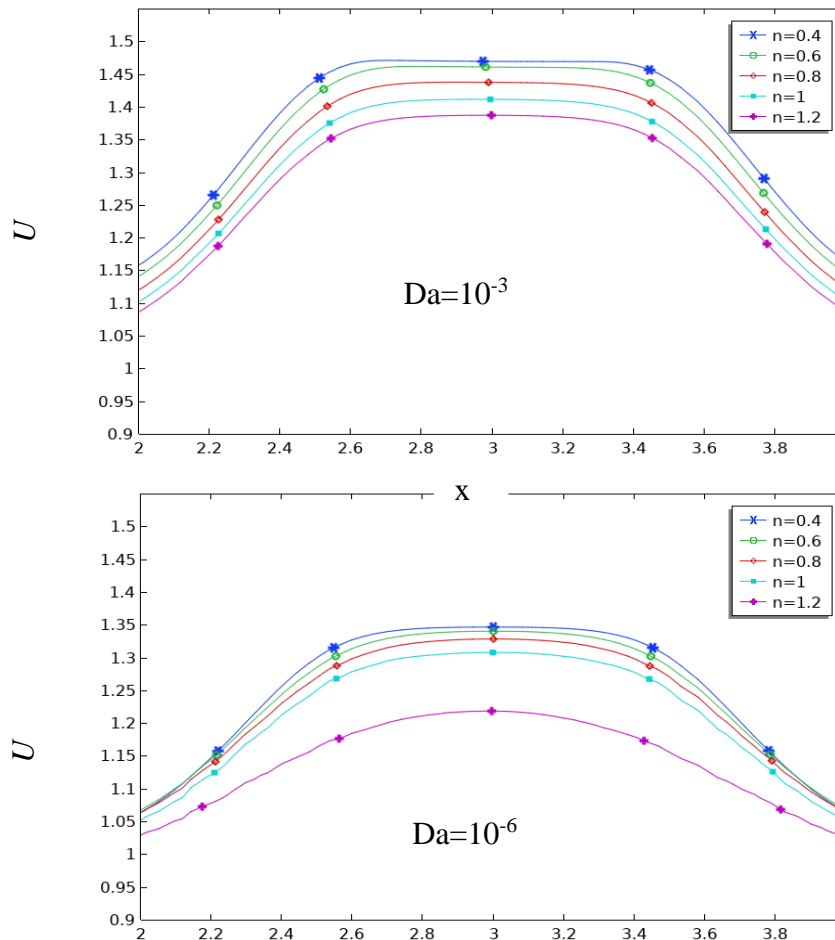


Figure 6: Variation of x-component velocity (U) with x for selected n ($Pr=70$ et $Re=50$, $B=0.75$, $Br=0$)

Fig. 6 gives the variation of the horizontal component of velocity along the median plane ($y=0.5$) for different n . Tracing is reduced to the narrowed part of the channel ($2 \leq x \leq 4$). Two values of Darcy numbers are used, namely 10^{-3} and 10^{-6} . For a fixed power index, figure 6a (for $Da=10^{-3}$), shows that fluid velocity increases once it enters the narrowed part of the channel. This increase is certainly due to the Venturi effect inducing an acceleration of the fluid accompanied by a decrease in pressure. This figure reveals also that an increase in n is accompanied by a decrease in the velocity of the fluid in the convergent and that consequently the venturi effect becomes less pronounced for shear-thickening fluids.

Indeed, for the same shear rate, an increase in n (transition from thinning to thickening character) induces an intense increase in the fluid apparent viscosity, mainly close to the walls of the convergent where the shear rate is moderately high. This behavior results in an intensification of the drag forces exerted on the fluid from the porous solid matrix and the walls of the enclosure. Consequently, fluid motion in the channel becomes more difficult, reducing its longitudinal velocity. The same phenomenon is observed and can be interpreted in the same way for $Da=10^{-6}$, except that in this case we observe the effect of decreasing permeability impacting a significant reduction in the horizontal component of velocity. For $n=0.4$, the maximum dimensional velocity in the convergent zone (at $x=3$) is 1.47 for $Da=10^{-3}$ versus 1.34 for $Da=10^{-6}$. At low permeability ($Da=10^{-6}$), the shear-thickening effect is added to the decelerating effect of the porous matrix, leading to a more expressive decrease in fluid velocity in the convergent zone and a reduction in the venturi effect.

V.3. Effect of the Brinkman number

This part concerns the impact of the Brinkman number (Br) on Nu_m near active bottom channel walls as well as on S_T . The Prandtl, Reynolds and Darcy numbers are fixed at 100, 50 and 10^{-3} respectively. The cavity expand ratio B is invariable and set to 0.5. Two power index values are used related to thinning and thickening fluid characters ($n=0.4$ and $n=1.4$). The Brinkman number is varying from 0 to 1. Fig. 7 shows the variation of S_T and Nu_m with Brinkman number for shear-thinning fluid ($n=0.4$).

As shown in Fig.7, total created entropy is maximal in the absence of viscous dissipation ($Br=0$), then decreases as the Brinkman number increases.

Parallel and in the same way, we observe a slight decrease of almost 1.3% in the average Nusselt number as Br increases from 0 to 1. In fact, for $Br = 0$, as the cold fluid enters the porous channel two heat flows from the hot upper and lower walls of the channel induces the fluid to heat up and simultaneously increase in temperature.

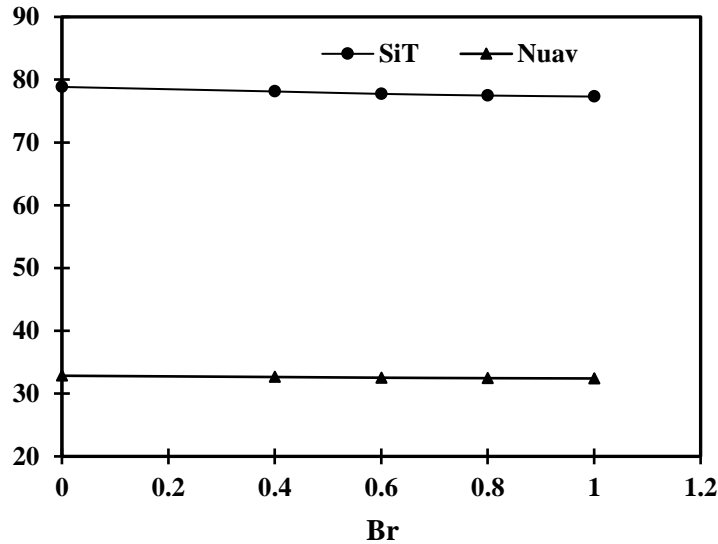


Figure 7: Total entropy production and average Nusselt number Vs Br ($n=0.4$)

In this context, heat transfer between the hot walls of the porous channel and the fluid decreases progressively. The fluid tends toward a thermal equilibrium state with the active walls of the channel, depending on Re , Da and the pipe length. An increase in the Brinkman number causes in intrinsic heating inside the fluid as a result of viscous dissipation effects. Heat transfer between active walls and the fluid is less intense in this case, leading to a reduction in thermal gradients and consequently in Nu_{av} and S_T . It should be noted that the irreversibility decrease for shear-thinning fluid is insignificant and that in this case we count a 2% reduction in total entropy generation when Br goes from 0 to 1. This can be interpreted by a weak effect of viscous dissipations following a reduction in the apparent dynamic viscosity of the fluid. To more explain this result, we have plotted in figure 8 the variation of the temperature at the center line of the flow versus x (for $y=0.5$). As it can be seen, once inside the channel, the fluid temperature increases in the wide left-hand and right-hand channels and practically stabilizes in the adiabatically narrowed section.

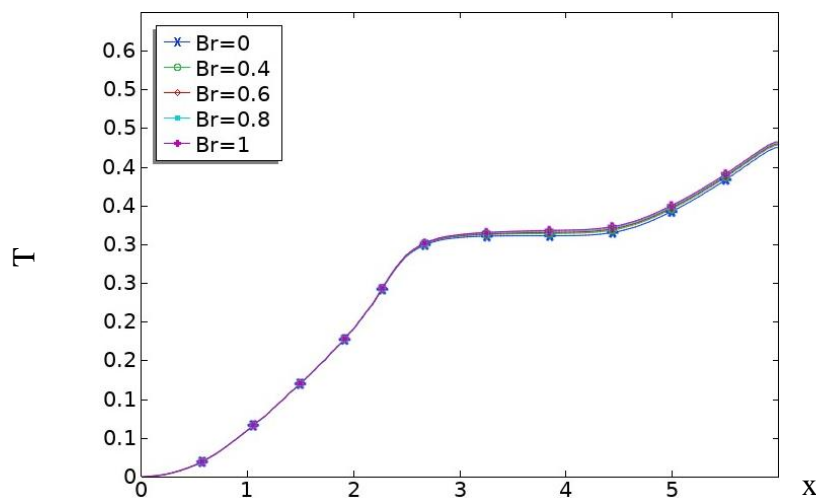


Figure 8 : Variation of the fluid temperature at the center line of the flow with x ($y=0.5$ and $n=0.4$)

Figure 8 shows that an increase in Br tends to a slight raise in the fluid temperature, and consequently in its internal thermal energy. As a result, heat transfer between the fluid and the hot walls of the channel is reduced, leading to a decrease in thermal gradients and, consequently, in both the average Nusselt number and total entropy production.

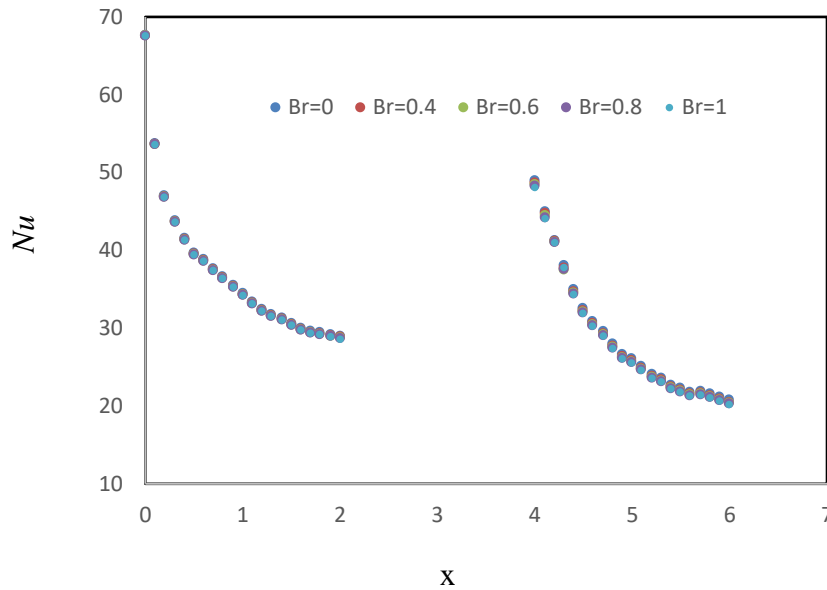


Figure 9 : Local Nusselt number variation (Nu) with x for different Br ($n=0.4 ; B=0.5$)

Figure 9 illustrates the change in the local Nusselt number near the lower active walls of the channel for $n=0.4$. From this figure one can note that local Nusselt number exhibits a discontinuity along the adiabatic walls, it takes a maximum value at the entrance to the left active compartment and then decreases until it reaches its end. These observations indicate the existence of heat transfer between the active walls of the wide left-hand part of the channel and the fluid, which steadily decreases as the fluid approaches the constriction and results in an increase in fluid temperature. In the adiabatically constricted section, where there is no heat transfer, the fluid temperature is kept virtually constant. Once the fluid reaches the right-hand active compartment, local Nusselt number resumes practically the same variation as for the left-hand compartment, giving rise to the same interpretations.

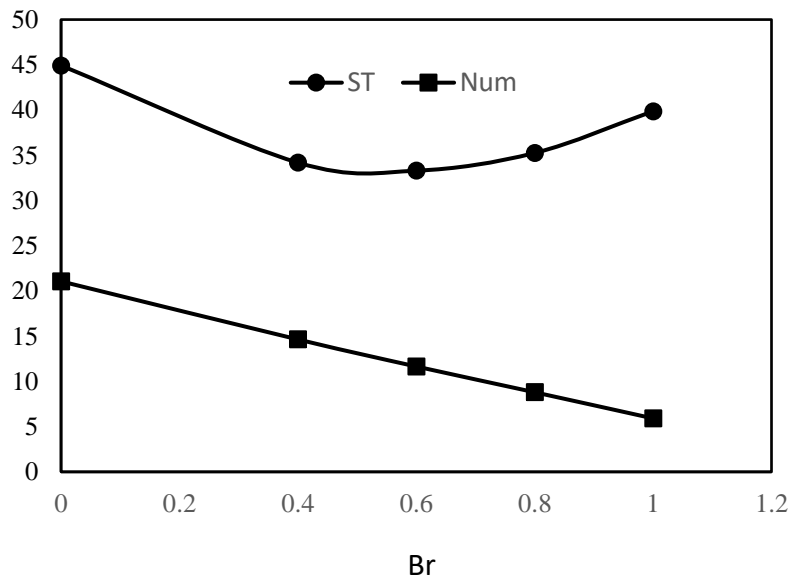


Figure 10: Total entropy generation and average Nusselt number Vs Br ($B=0.5, n=1.4$)

Evolution of S_T and Nu_m versus Brinkman number is exhibited in Fig.10 in the case of shear-thickening non-Newtonian fluid ($n=1.4$). Similar situation to the previous case is obtained, related to the

average Nusselt number variation with the Brinkman number. In this case ($n=1.4$) the diminution of Nu_m is more pronounced, and we count a decrease by almost 70% as Br grows from 0 to 1. This is mainly due to an increase in the thermal internal energy of the fluid, which raises its temperature and thus reduces heat transfer between the channel active walls and the fluid. The most significant anomaly concerns the behavior change in total thermal created entropy as a function of Br, which consists of a decrease followed by an increase, passing through a minimum value for Br close to 0.5.

First of all, many authors point out that variations in entropy production and Nusselt number are qualitatively similar, since both quantities involve thermal gradients. This observation, which seems reasonable in general terms, has exceptions related to specific physical phenomena, such as viscous dissipation. In fact, the increase in entropy production can be explained by a reversal of heat transfer. As shown in figure 11 illustrating the variation of temperature at the median plane ($y=0.5$) for different Brinkman numbers, the fluid temperature in the right-hand wide compartment is higher (for $Br=1$) than the temperature of the hot wall indicating a reversal of heat transfer from the fluid to the hot wall of the channel, characterized by negative thermal gradients. On the other hand, in the left-hand hot compartment, the fluid temperature is significantly lower than active wall, reflecting heat transfer from the hot wall to the fluid, characterized by a positive Nusselt number. In this case, we can conclude that that a reversal heat transfer can lead to a reduction in the average Nusselt number and, on the other hand, to an increase in entropy production.

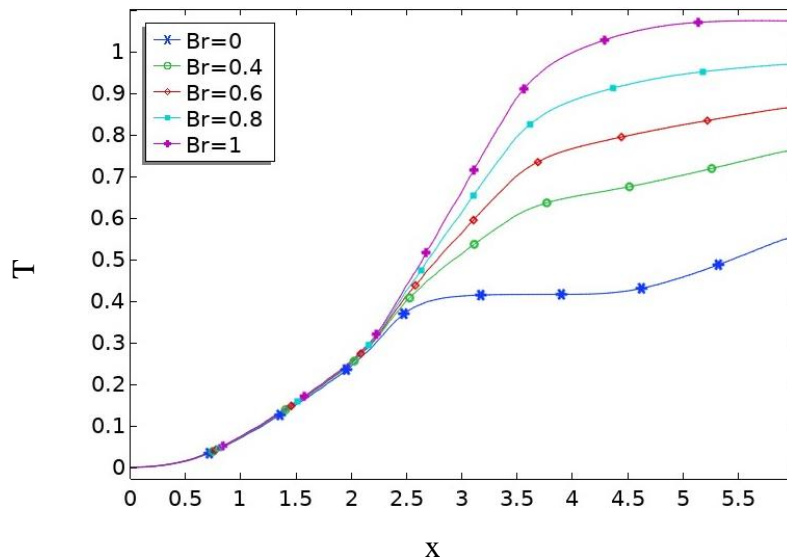


Figure 11: Variation of the fluid temperature with x at $y=0.5$
($n=1.4$, $B=0.5$)

The temperature of the fluid calculated at the median plane ($y=0.5$) increases as it flows through the wide left-hand part of the channel, without any observed influence of viscous dissipation. A bifurcation point, warning of Brinkman effect, appears very close to the entrance of the channel, from which the median temperature continues to rise. In this region and because of the venturi effect, velocity gradients increase considerably, amplifying the source term in the heat equation. Added to this extrinsic cause is an intrinsic effect due to the increase in the Brinkman parameter. These two cooperating causes will give rise to relatively high viscous dissipation. As a result, the source term in the heat equation becomes significant, leading to a considerable increase in fluid temperature.

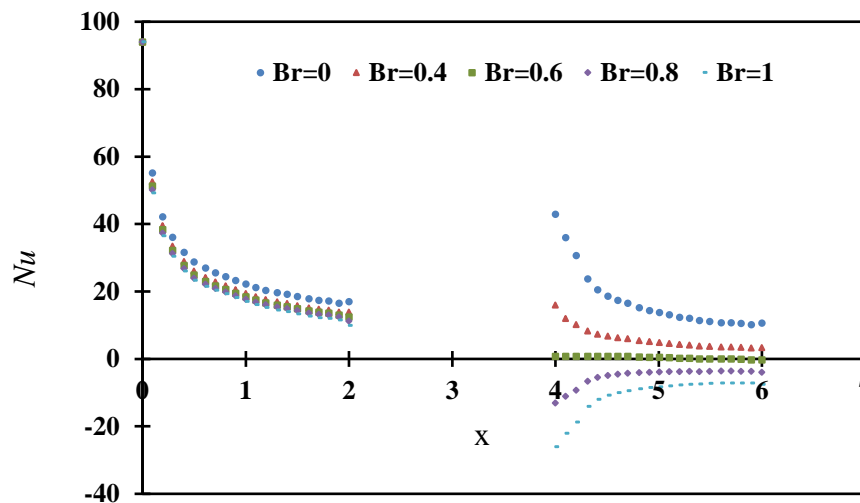


Figure12 : Local Nusselt number (Nu) evolution with x for different Br ($n=1,4$; $B=0.5$)

To clearly visualize this inversion of heat transfer, the local Nusselt number on the hot walls of the left and right wide pipes is plotted in figure12. As observed, Nu decreases at the two active walls ($0 \leq x \leq 2$ and $4 \leq x \leq 6$) for Br below 0.8 translating heat transfer from the walls to the fluid. From $Br=0.8$ onwards, Nu remains positive on the left-hand hot wall whereas it becomes negative as soon as the fluid enters the right-hand wide compartment, indicating a reversal in the direction of heat transfer. In this case, the fluid heats up in the wide right-hand compartment by convective effect, then re-enters the narrowed channel, where it heats up this time by viscous dissipation due to the increase in its velocity and Brinkman number. The temperature of the fluid exceeds that of the walls, reversing the direction of the thermal gradients.

VI Conclusion

Thermodynamics irreversibility and heat transfer for a non-Newtonian fluid with viscous dissipation effect in mixed convective flow in a horizontal porous channel with singularity was numerically studied. The set of governing equation, written under extended Darcy -Forchheimer formulation, is solved using COMSOL software. The model of power index is used. The main results found are summarized in the following points:

1. For constant B, Nu_m is maximal for shear-thinning fluid ($n=0.4$). Nu_m decreases as n rises and tends towards a minimum value at high n .
2. For expand ratio $B=3/4$, the reduction in the production of thermal entropy is 66% when n varies from 0.4 to 1.8.
3. The influence of the expand ratio B on Nu_m and S_T is highly significant for shear-thinning fluid, slight for Newtonian fluids and almost absent for shear thickening fluids ($n>1$).
4. The decrease in entropy production is about 12%, 2% and 0.7% for a power index equal to 0.4, 1 and 1.8 respectively when the aspect ratio is increased from 0.25 to 0.75.
5. As Darcy number increases, effect of power index on Nusselt number becomes more important. A decrease in Nu as the power index increases is observed.
6. Results show that the greater the Da, the greater the decrease in Nu , when n increases.
7. Effect of Da is more significant for shear-thinning fluids. Results reveal an increase in created entropy of almost 70% for $n=0.4$ versus 50% for $n=1.2$ when Da is increased from 10^{-6} to 10^{-3} .
8. The irreversibility and heat transfer decrease for shear-thinning fluid are insignificant. We count a 2% reduction in total entropy generation when Br goes from 0 to 1 for $n=0.4$.
9. For shear-thickening fluid ($n=1.4$) the diminution of Nu_m is more pronounced, and we count a decrease by almost 70% as Br grows from 0 to 1.
10. Behavior of total created entropy with Br changes in the case of shear-thickening fluid. It consists of a decrease followed by an increase, passing through a minimum value for Br close to 0.5.
11. The increase in entropy production, at relatively high Brinkman number, is the result of a reversal in the direction of heat transfer.